JOC The Journal of Organic Chemistry

Article

pubs.acs.org/joc

Examination of the Reactivity of Benzoxaboroles and Related Compounds with a *cis*-Diol

John W. Tomsho† and Stephen J. Benkovic*

Department of Chemistry, Penn State University, 414 Wartik Laboratory, University Park, Pennsylvania 16802, United States

Supporting Information

ABSTRACT: Benzoxaboroles have been emerging as an interesting and useful scaffold in drug discovery due to their apparently unique reactivity toward diols under physiological conditions. In this work, the reaction of benzoxaborole with the diol-containing, fluorescent dye Alizarin Red S is probed. Steady-state and presteady-state experiments have been conducted for the characterization of the reactions over a wide range of pH. Results indicate that Alizarin Red S reacts with both the boronic (neutral, trigonal) form as well as the boronate (anionic, tetrahedral) form of benzoxaborole in a reaction largely analogous to that previously determined for the simple phenylboronic acid. However, in certain key aspects, the reactivity of the benzoxaborole was found to differ from that of simple phenylboronic acid. The structural origin of these differences has been explored by examination of compounds related to both benzoxaborole and phenylboronic acid. These results may be applied to rational drug discovery efforts aimed at expanding the use of benzoxaboroles in medicine.

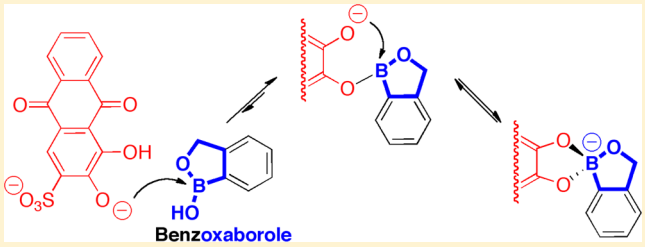

INTRODUCTION

During most of the 55 years since their discovery,[1] the benzoxaborole heterocycle (**1**) has received little attention until recently. This heterocycle consists of a phenyl ring fused with a five-membered cyclic boronate termed an oxaborole. Indeed, other oxaborole-containing compounds are already finding applications in drug discovery[2] and synthetic protocols.[3] The benzoxaboroles in particular have been found to possess high water solubility and resistance to hydrolysis,[4] excellent sugar (diol) binding under physiologically relevant conditions,[5,6] and a low pK_a compared with that of simple phenylboronic acid.[7] Of particular interest, the use of the benzoxaborole scaffold in drug discovery has been on the rise.[8,9] To date, these compounds have found use as inhibitors of Leu-tRNA synthetases (for antifungal,[10] antibacterial,[11] and antitrypanosomal agents.[12,13]), phosphodiesterase-4 (PDE-4, anti-inflammatory),[14] β-lactamase,[15] and several antibacterials.[11]

In addition, this scaffold has been recently found to have several applications in biotechnology including incorporation into polymeric materials for sugar-responsive insulin delivery[16] and mediating the delivery of a protein toxin to the cytosol.[17] In general, the benzoxaborole scaffold has been selected time and again for its enhanced reactivity or binding to target diols whether on the cell surface or in the active site of an enzyme. In this work, we attempt to answer the question "What properties of this scaffold are responsible for its unique reactivity?".

To answer this question, the reactivity of a benzoxaborole (**1**) with a model diol Alizarin Red S (**ARS**) in aqueous solution has been examined in both the steady-state and presteady-state. **ARS** was chosen as a model system since it has several desirable characteristics including: fluorescence and UV/vis spectral differences arising upon reaction with boronic acids, ready reaction with boronic acids in neutral, aqueous solution, and a low pK_a that resembles "biological" nucleophiles. The reaction and its products have been characterized across a wide range of pH of approximately 4−9. The results of these experiments are compared with those recently determined with the simple phenylboronic acid (**PBA**, **4**)[18] in order to elucidate any key mechanistic differences between the two systems. Finally, related compounds (Figure 1) with altered heterocyclic ring systems (**2** and **3**) or altered pK_a via ring substitutions (**5** and **6**) have been examined to assess the cause of any differences.

In general, it is found that benzoxaborole reacts with Alizarin Red S with a mechanism analogous to that determined for phenylboronic acid.[18] The reaction proceeds preferentially at near neutral solution pH via a sequential two-step reaction in which a bimolecular esterification is followed by an intramolecular cyclization resulting in a diester spiro adduct. The unique reactivity of the benzoxaborole heterocycle arises from the kinetic contributions of the cyclization reaction. This enhanced cyclization appears to arise from the contributions of the five-membered oxaborole heterocycle.

RESULTS AND DISCUSSION

Steady-State Analysis. The investigation of the reaction between **1** and **ARS** was begun by examining the individual reactants as well as the products of the spontaneous reaction that occurs in buffered aqueous solution via spectrophotometric methods. In all cases reported in this work, Good buffers,

Received: October 24, 2012
Published: November 1, 2012

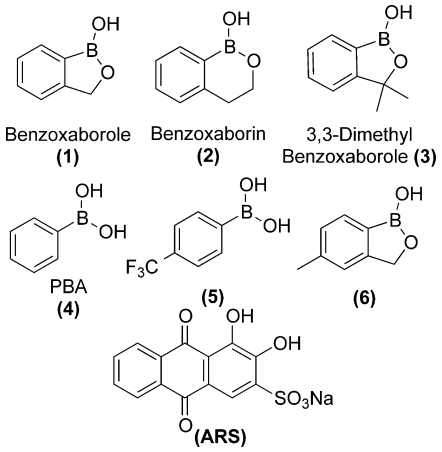

Figure 1. Compound structures and designations.

versus other common buffers such as Tris or phosphate, were chosen due to their previously determined unreactivity toward boronic acids.[18] Solution pH was varied from approximately 4 to 10 with buffers while extremes of pH, 1 and 13, were achieved with dilute HCl and NaOH solutions respectively. The UV/vis spectra of the compounds illustrated in Figure 1 and the product of the **1:ARS** reaction were taken at each pH studied. Utilizing the method of Tomsho, et al,[7] pK_a determinations were made (the data for **1**, **ARS**, and **1:ARS** are reported in the Supporting Information) and the results are summarized in Table 1. Of particular note is the finding that

Table 1. pK_a Values Determined by UV/Vis Spectral Titration[a]

compound	pK_a
1	7.3[b]; 7.7[c]
2	8.4[b]
3	8.3[b]
4	9.1[b]; 9.2[c]
5	8.4[b]
6	7.6[b]
ARS	6.0, 11.0[c]
1:ARS adduct	4.6, 9.5, 11[c]

[a]The pK_a determinations were achieved by the method of Tomsho, et al.[7] which also reported the pK_a of **1**–**3** and **6** with a lesser concentration of DMSO in the final solution than those utilized herein. DMSO was used to prepare high concentration stock solutions of compounds **1**–**6**. These data are reported here for ready comparison. [b]0.5% v/v DMSO. [c]4% v/v DMSO.

two of the observed pK_a's for the **1:ARS** adduct differ significantly from those measured for **1** and **ARS** individually while the highest (11) is an exact match for the second alcohol deprotonation of "free" **ARS**. The interpretation of this finding is that under conditions of pH ≤ 10 the reaction equilibrium lies to the right and the product spectra are being observed, while at high pH the reaction equilibrium lies to the left and the spectra are reflective of the reactant.

Fluorescence characterizations were subsequently pursued and it was found that none of the boronic acid compounds under study exhibited significant intrinsic fluorescence. Both **ARS** and the **1:ARS** adduct exhibited fluorescence across a wide range of pH as is shown in Figure 2. At the pH of maximum fluorescence, between pH 6.5 and 7.0, a nearly 100-

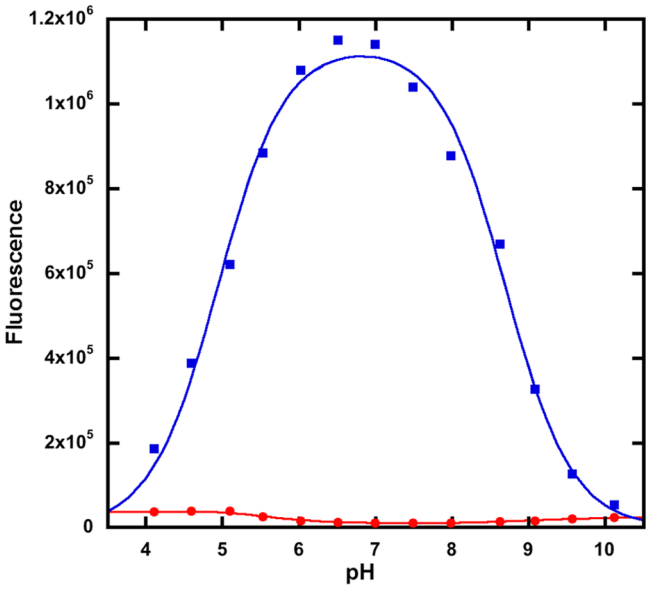

Figure 2. Fluorescence vs pH for **ARS** (●) and **1**:**ARS** (■). Excitation was at 440 nm while emission was monitored at 565 and 585 nm respectively. The fluorescence at pH = 1 and 13 was similar and small for both solution sets and was not shown for clarity. Data for **1**:**ARS** were fit to a two-pK_a equation, eq 1, and resulted in pK_a's of 4.9 and 8.7.

fold enhancement in fluorescence is observed for the **1:ARS** adduct when compared to **ARS**. The spectra for the **1:ARS** adduct from pH 4 - 9 exhibit unchanging wavelength maxima, 440 ± 5 nm excitation and 585 ± 5 nm emission, across pH indicative of a single, major fluorescent species (Data not shown). This adduct species exhibits a red shift in the emission maxima, when compared with **ARS** (565 nm), consistent with extended conjugation of the pi system. The resulting fluorescence vs pH curve can be fit by eq 1. This equation describes a linear reaction in which three species are interconverting in a pH dependent manner with the middle species solely contributing the fluorescence signal. The resulting pK_a values obtained by the fitting of this data are 4.9 ± 0.1 and 8.7 ± 0.1. These results may be compared with those obtained from UV/vis methods and it is found that the values obtained from the two methods are similar. Any differences noted may be due to the fact that the fluorescent measurements are heavily biased toward the product contributions with their much higher signal relative to the reactants.

$$[\text{Fluorescent Species}] = \frac{[\mathbf{ARS}]_T \times 10^{(pK_{a2}-pH)}}{1 + 10^{(pK_{a2}-pH)} + (10^{(pK_{a1}-pH)} \cdot 10^{(pK_{a2}-pH)})} \quad (1)$$

Equation 1 describes a model where three species are in an equilibrium connected by two ionizations with only the middle species contributing to the fluorescent signal. It is assumed that the fluorescence signal is directly proportional to the concentration of the fluorescent species, [Fluorescent Species]. The equation is placed in terms of the total concentration of **ARS**, $[\mathbf{ARS}]_T$, observed ionization constants (pK_{a1} and pK_{a2}), and solution pH.

The properties of the fluorescent species were further characterized with fluorescent lifetime measurements taken

dx.doi.org/10.1021/jo302264g | J. Org. Chem. 2012, 77, 11200–11209

from pH 4−10. Consistent with the previous results, two species were detected with one species accounting for 82−88% of the fluorescent signal from pH 4−9. The major fluorescent species' lifetime varies from 0.49−0.64 ns while the minor species' lifetime was 2.49−2.05 ns as pH is varied from 4 to 10. These data also reveal that the major fluorescent species undergoes a change in lifetime from 0.49 ns at pH = 4 to 0.64 ns at pH 6−10, likely corresponding to the observed **1:ARS** adduct pK_a of 4.6−4.9. From pH 6−8, both relative fluorescent contributions and lifetime measurements are unchanging. At high pH, an explanation for the observed loss of fluorescence may be found. Over a pH of 8−10, the lifetime of the minor species changes from 2.36 to 2.05 ns respectively. Additionally, the relative contribution to fluorescence of the major species drops from 87 to 66% as pH is increased from 9 to 10. Taken together, these data are indicative of another ionization step in which the highly fluorescent adduct species is transitioning to a species with much less fluorescence as a function of pH. This finding reinforces the validity of the **1:ARS** adduct pK_a of 8.7−9.5 from the fluorescence and UV/vis spectral data, Figure 2 and Table 1, respectively.

Since useable fluorescence signal changes were noted after the reaction between **1** and **ARS** in solution at near neutral pH, steady-state titrations with fluorescence detection were executed. Using a fixed, low concentration of **ARS**, 20 μM, solutions were prepared such that the concentration of **1** was varied from 0 to 10 mM. After a fixed incubation period, the change in fluorescence of the solution was measured and plotted against total [**1**] (Figure 3). The data were fit with eq 2

Table 2. Comparison of the Association Constants for 1 and ARS as Determined by Three Methods at Various pH Values

	K_a (M^{-1})		K_{a1} (M^{-1})	K_2
pH	fluorescent titration[a]	ITC[a]	kinetics[b] (k_{on}/k_{off})	^{11}B-NMR[c]
5	690 ± 30	480 ± 20	420 ± 180	0.40 ± 0.04
6	2580 ± 90	2030 ± 80	1140 ± 200	0.70 ± 0.05
7	3190 ± 110	3390 ± 420	1950 ± 480	0.87 ± 0.04
8	1140 ± 40	780 ± 30	840 ± 100	ND[d]
9	100 ± 10	ND[e]	170 ± 25	ND[d]
10	ND[e]	ND[e]	ND[e]	0.12 ± 0.03

[a]Overall K_a values are calculated based on the total concentration of **1** at each pH and are expressed in units of M^{-1}. [b]Values are calculated by dividing the observed k_{on} by k_{off} from the kinetic progress curves at each condition of pH. [c]K_2 values (unitless) calculated based on ^{11}B-NMR experiments as described previously.[18] [d]Under these conditions of pH, significant peak overlap precluded accurate integration. [e]Binding under these conditions provided too low a signal to allow for accurate measurement; ND = not determined.

to determine the binding constants and the results are summarized in Table 2.

$$\Delta\text{Fluorescence} = \frac{[B]_T \times \text{Fluor}_{max}}{(1/K_a) + [B]_T} \quad (2)$$

Equation 2 describes the K_a determination by two-component fluorescent titrations; ΔFluorescence is the observed change in fluorescence, $[B]_T$ is the total concentration of boron species, and Fluor_{max} is the maximum change in fluorescence.

Isothermal titration calorimetry (ITC) was then used to examine stoichiometry of binding and to determine true

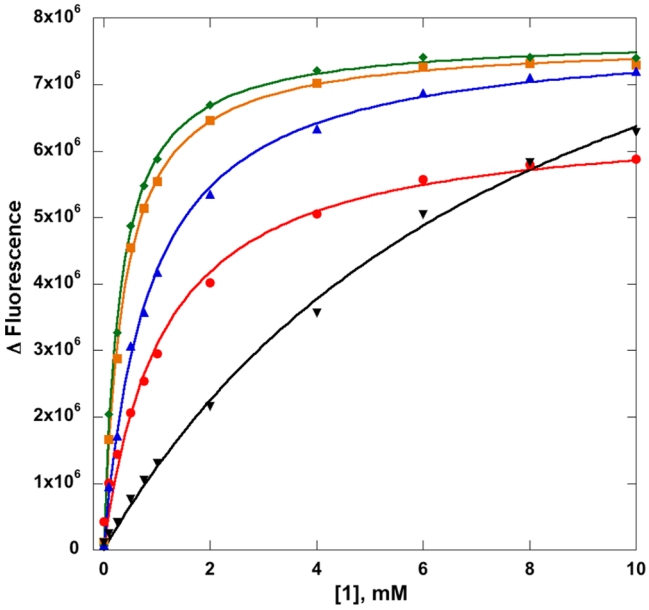

Figure 3. Steady-state fluorescent titration of **ARS** with **1** for the determination of the association constant at pH 5 (red ●), 6 (orange ■), 7 (green ◆), 8 (blue ▲), and 9 (▼). [**ARS**] = 20 μM while $[\mathbf{1}]_{total}$ was varied from 0 to 10 mM. Results of fitting to eq 2 are indicated in Table 2.

thermodynamic binding constants. Reactions were set up at each pH from 5 to 10 with a solution of **1** being titrated into a solution **ARS** in the receiving cell. The buffer composition and DMSO percentage were matched in both solutions to minimize background heats of dilution. In addition, the heat of dilution of **1** was measured and used as a baseline for the reaction measurements. Across all pH conditions examined, 1:1 binding between **1** and **ARS** was found. A representative titration curve and binding constant determination is shown in Figure 4. The binding constants measured with this method are reported in Table 2 and are found to closely match those determined by the fluorescent titration method. These findings then are useful for consideration of the overall reaction within this system for the transition from reactants to all potential products.

In our previous work with phenylboronic acid,[18] ^{11}B NMR was found to be an extremely useful tool and provide important information about the reaction equilibrium. This method is of use because of its sensitivity to the changes in the configuration about the boron atom in solution. Specifically, it allows the independent measurement of the diester, spiro product that is tetrahedral about the boron atom due to its distinctive chemical shift. The structure of this product is illustrated in Figure 5 and is labeled as the **NMR Adduct** since its exclusive contribution to the reaction may be measured via this technique. The NMR spectra thus obtained reveal two unique peaks, one from all of the boron-containing species in rapid equilibrium (i.e., free **1** and the **Fluorescent Adduct** shown in Figure 5) and the other from the slowly exchanging **NMR Adduct**. The data obtained from the integration of these peaks is then used to calculate K_2. The data and K_2 calculations are shown in the Supporting Information. Tabulated results are found in Table 2.

Inspection of these data immediately revealed that the reaction of this system must proceed through a two-step mechanism such as that depicted in Figure 5. In this reaction, the first adduct formed is the result of a single dehydration step while a second dehydration must occur to form the diester,

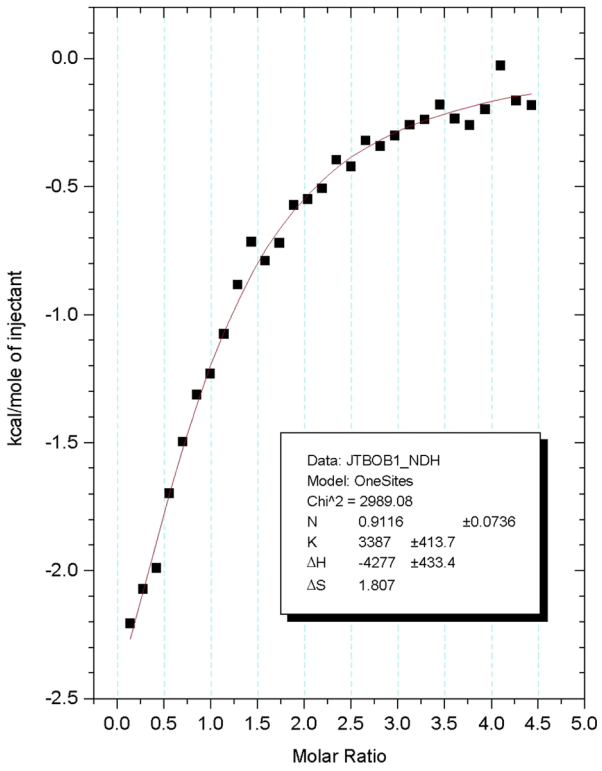

Figure 4. Isothermal titration calorimetry of the reaction of **1** with **ARS** at pH 7. Data fits well to a one-site binding model resulting in K_a = 3390 ± 420 M^{-1}, ΔH = −17.9 ± 0.2 kJ/mol, ΔS = 7.57 J mol^{-1} K^{-1}, and ΔG = −20.2 ± 0.2 kJ/mol.

spiro adduct. The overall binding, as determined by either fluorescence titrations or ITC, between **1** and **ARS** to yield all products reaches its maxima between pH 6 and 7. These findings are consistent with the preferred reaction occurring between a singly deprotonated **ARS** (pK_a = 6.0) and the neutral, trigonal form of **1** (pK_a = 7.7). Additionally, the K_2 data show that at pH 7, the molar ratio of the two products depicted in Figure 5 is nearly 1:1 yet the fluorescent lifetime experiments tell us that one of these species is responsible for over 80% of the observed fluorescence. The first adduct is assigned as the species with the greater fluorescence due to the presence of a trigonal boron species with its planar geometry and empty p-orbital that act to extend conjugation.[19−21] With a nonplanar structure and a boron atom with a filled p-orbital, the diester spiro product is assigned as the product yielding the lesser contribution to fluorescence. The opening of the oxaborole ring was also considered at this juncture however no evidence was found to conclusively support the existence of a ring-opened intermediate. Additionally, the pK_a of a diester, ring-opened adduct structure would likely be extremely low (<5) hence the neutral, trigonal planar form would not be a significant contributor with solution pH from 5 to 9 when the fluorescence is most intense.

Thus far, steady-state examinations have revealed important information about the nature of the reaction in question: (1) UV/vis spectral analyses have elucidated the ionization constants of the reactants and major products, (2) titrations have characterized the thermodynamics of the overall reaction, (3) ^{11}B NMR has allowed us to conclude that the reaction proceeds in two sequential steps and to quantitate the contribution of one of the product species, and (4) examination of the fluorescent lifetime data combined with the application of chemical insight has allowed us to assign the likely structure of the major contributor to fluorescence to a structure that is trigonal about boron with empty p orbitals and a planar structure that provides a system with extended conjugation. Yet there is a dearth of data that characterize the initial phase of the reaction between **1** and **ARS**. For this information, we turn to studies of the reaction in the presteady-state.

Presteady-State Analysis. Reaction kinetics were monitored using a stopped-flow apparatus with fluorescence detection. Solutions of **1** and **ARS** were prepared in matched buffer solutions (buffer strength, [DMSO], etc.) from pH 4 to 9.5. The concentration of **ARS** was fixed and limiting (100 μM final) while **1** was varied in excess (1−4 mM final). The reaction was initiated with rapid mixing of the two solutions. The resulting fluorescence progress curves were fit to a single exponential and the apparent rates were plotted versus [**1**]. Linear fitting of these data yield the formation and dissociation rates, via the slope (k_{on}) and y-intercept (k_{off}) respectively, for the reactions at each pH. The k_{on} and k_{off} data are plotted versus pH and shown in Figure 6.

The analysis of these data was begun by the calculation of the K_{a1} values at each pH. This was achieved by simply dividing the value of k_{on} by k_{off} for each condition of pH and the results of selected conditions are recorded in Table 2. Of note is the difference between the overall binding constant, K_a, and the kinetic binding constant, K_{a1}. This difference can be explained by the two-step sequential reaction mechanism depicted in Figure 5. In this case, the overall K_a reflects the total of all products formed while K_{a1} and K_2 reflect the formation of the monoester adduct and its partitioning to the diester, spiro adduct respectively. Given this relationship, eq 3 has been derived and used as confirmation of the proposed mechanism.

$$K_a = K_{a1} + K_{a1} \times K_2 \quad (3)$$

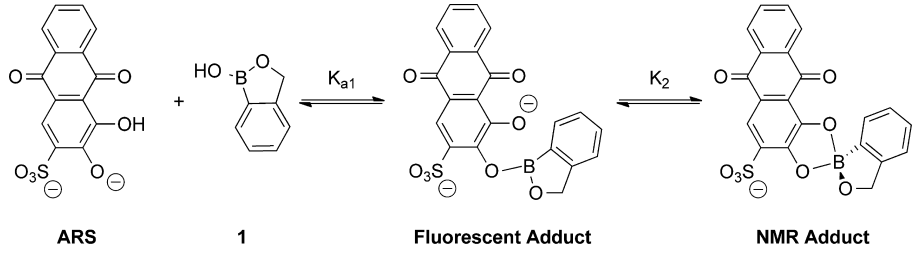

Figure 5. Minimal mechanism for the reaction of **1** with **ARS** based on experimental results from the steady state at near neutral pH's. The Fluorescent Adduct structure is assigned as the major source of the detected fluorescence signal while the NMR Adduct is that which can be independently measured via its unique peak in ^{11}B NMR. Such a mechanism accounts for the observed difference of the K_a's from kinetic (K_{a1}) and thermodynamic (overall K_a and K_2) measurements via eq 4.

dx.doi.org/10.1021/jo302264g | J. Org. Chem. 2012, 77, 11200−11209

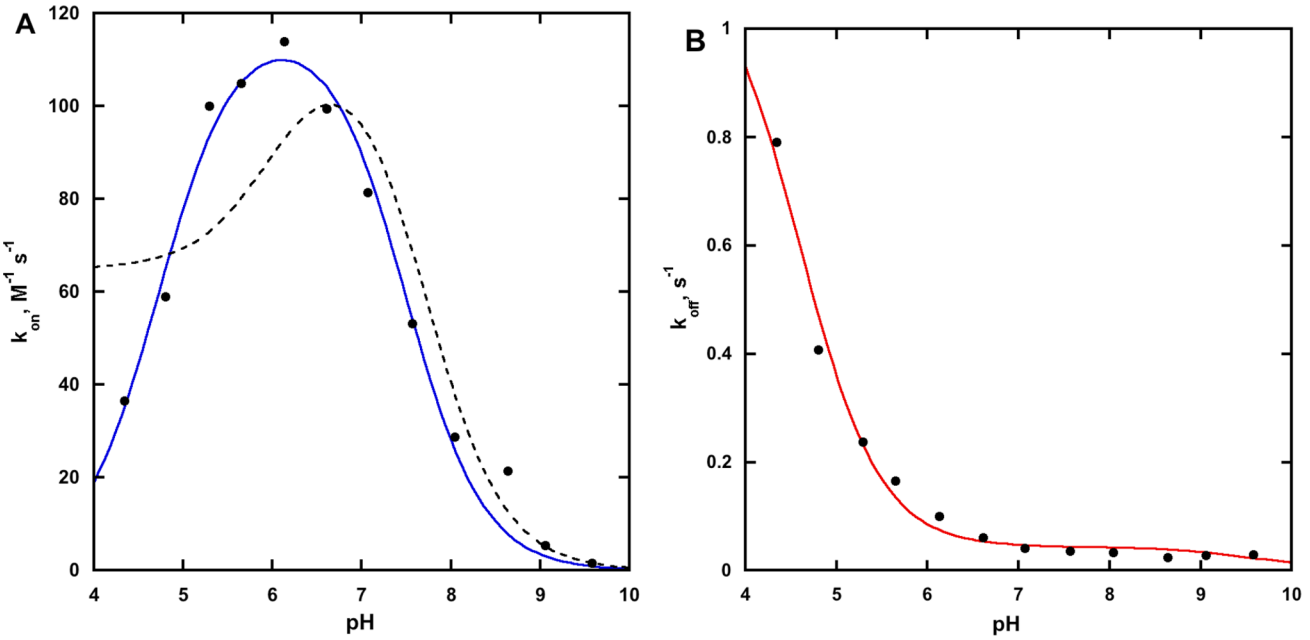

Figure 6. Analysis of pH profiles of k_{on} and k_{off} obtained from stopped-flow experiments enable partial mechanism elucidation: (A) forward rate data (k_{on}) are fit to eq 4 (dashed, black line) and a two-pK_a equation (solid, blue line) in the same form as eq 1 as an approximation since an exact solution for the mechanism cannot be solved, apparent pK_a's are 4.7 ± 0.1 and 7.5 ± 0.1; (B) reverse rate data (k_{off}) are fit to eq 5.

The sequential two-step mechanism found in effect with benzoxaborole, **1**, is identical in form to that previously determined with phenylboronic acid, **4**.[18] Other similarities between the two systems include: UV/vis and fluorescence spectral properties; pH profiles of fluorescence and binding, once the altered pK_a of **1** is taken into account; and the apparent preference for the reaction to occur between the singly deprotonated **ARS** and the neutral, trigonal form of **1**. Therefore, an analogous reaction mechanism is proposed.

It is seen that **ARS** may exist as any of three species, from the fully protonated A_0 to the monodeprotonated A_1 to the fully deprotonated A_2. These ionization steps are connected by the equilibria K_1^A and K_2^A respectively. B_1 and B_2, connected by the equilibrium K_1^B, represent the neutral, trigonal and anionic, tetrahedral forms of **1**, respectively. The reactions between the various ionization states of **ARS** and **1** may then proceed via three parallel, single-step reaction paths to form intermediate products P_1, P_2, and P_3. Each of these intermediate products represent a differing ionization state of the monoester adduct of **1:ARS** and they exist in rapid equilibrium with the others as dictated by solution pH and K_1^P and K_2^P. These products may then undergo a second, intramolecular attack to form the cyclic, diester product P_4 that contains an anionic, tetrahedral boron atom.

With an essentially identical format of the mechanistic proposal for the reaction between **1** and **ARS** as was determined for the reaction with **4**, the previously determined[18] rate equations for k_{on}, eq 4, and k_{off}, eq 5, versus pH were evaluated for compatibility with this system. The equations were modified to reflect the revised numbering of the steps used in Figure 7 and the pK_a values found for this system in independent measurements from the steady-state for **1** (pK_1^B), **ARS** (pK_1^A, pK_2^A), and the **1:ARS** complex (pK_1^P, pK_2^P). As can be seen in Figure 6 **B**, eq 5 provides an excellent fit to the k_{off} vs pH data. The k_{-1}, k_{-2}, and k_{-3} values obtained from this fitting are recorded in Figure 7.

$$\frac{k_{obs}}{[B]_T} = \frac{\nu}{[A]_T[B]_T} = k_1\left(\frac{[H^+]}{K_1^B + [H^+]}\right)\left(\frac{[H^+]^2}{[H^+]^2 + ([H^+]K_1^A) + K_1^AK_2^A}\right) + \left(\frac{k_2[H^+] + k_3K_1^B}{K_1^B + [H^+]}\right)\left(\frac{K_1^A[H^+]}{[H^+]^2 + ([H^+]K_1^A) + (K_1^AK_2^A)}\right) \quad (4)$$

Equation 4 describes the formation of the three monoester, adduct species, P_1, P_2, and P_3, from reactions between the various ionization states of **ARS** and **1**. pK_1^A, pK_2^A, and pK_1^B are fixed to 6.0, 11.0, and 7.7 respectively based on the results of the UV/vis determination of the pK_a's of **1** and **ARS**.

$$k_{obs} = \frac{\nu}{[P]_T} = \frac{(k_{-1}[H^+]^2) + (k_{-2}[H^+]K_1^P) + (k_{-3}K_1^PK_2^P)}{[H^+]^2 + ([H^+]K_1^P) + (K_1^PK_2^P)} \quad (5)$$

Equation 5 describes the dissociation of the three species, P_1, P_2, and P_3, that are connected by two ionization steps, K_1^P and K_2^P respectively. pK_1^P and pK_2^P are fixed to 4.6 and 9.5, respectively, based on the results of the UV/vis determination of the pK_a's of **1:ARS** adduct.

An inconsistency was noted when eq 4 was applied to the k_{on} vs pH data graphed in Figure 6A (dashed, black line). A reasonable fit was found for the right half (pH 6.5−9.5) of the graph where the contributions of the middle (A_1 + B_1) and bottom (A_1 + B_2) arms of the mechanism are controlling and the ionization of **1** is evident. At pH < 6.5, significant deviations between the data and the fit predicted by eq 4 were observed. In essence, eq 4 predicts a change in reaction rate, from the upper path (A_0 + B_1) to the middle path (A_1 + B_1), controlled by the ionization of A_0 to A_1 as represented by pK_1^A. These data

dx.doi.org/10.1021/jo302264g | J. Org. Chem. 2012, 77, 11200−11209

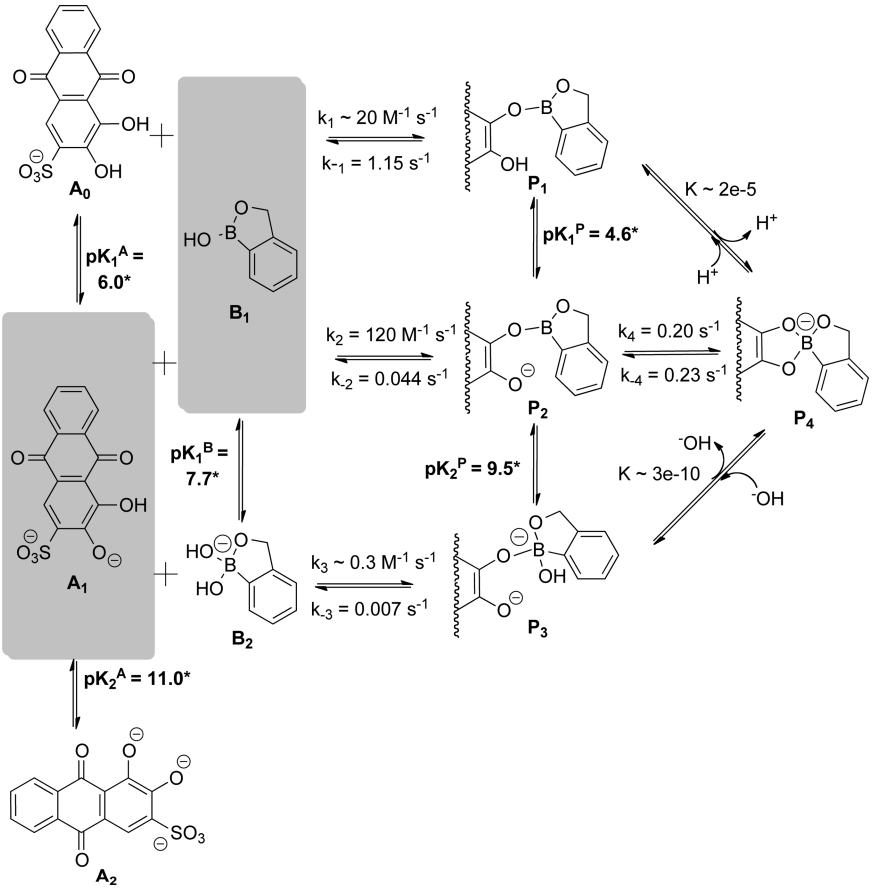

Figure 7. Proposed mechanism for the spontaneous reaction between **1** and **ARS** in aqueous solution as pH is varied from acidic (top) through near neutral (middle) to basic (bottom). Due to an inability to explicitly solve the necessary rate equations, values for k_1 and k_3 were estimated. *Values were determined in independent experiments.

indicate that the reaction is proceeding at low pH in a manner that is inconsistent with the independently determined pK_1^A = 6.0. In order to assess the extent of the deviation, the data are fit with a two-pK_a equation in the same form as eq 1 (solid, blue line). It is found that the right arm's apparent pK_a is 7.5 ± 0.1, a good match for the pK_a of **1**, and that the left arm's pK_a is 4.7 ± 0.1. This pK_a is strikingly similar to that found for the ionization of the products of the reaction under acidic conditions (P_1 to P_2 via pK_1^P).

With this finding, it is proposed that the observed deviation of the data from eq 4 may be explained by contributions from the product side of the reaction, that is, from pK_1^P and K_2. Attempts to derive equations for these models with the mechanism illustrated in Figure 7 proved exceedingly complex so the question was examined by modeling the reaction with the program KinTek Global Kinetic Explorer v.3.0. Indeed, it was found that the observed reaction progress curves, at pH 5 and 7, could be accurately simulated with a sequential two-step model given the experimentally determined rates of reaction (Supporting Information). Given a level of confidence in the model, the rates k_1, k_2, and k_3 are assigned the values given in Figure 7. The value of k_2 is the result of fitting eq 5 to the data from pH 6.0 to 9.5. This fit also yields a value for k_3 that is essentially zero. Given that all other steps in this lower reaction cycle are known, k_3 is calculated to be 0.3 M^{-1} s^{-1} via thermodynamic closure. The value for k_1 is approximated to be 20 M^{-1} s^{-1} via comparison of observed rates in Figure 6A and thermodynamic evaluation of the upper reaction cycle.

Subsequently, the second step of the reaction, the intramolecular attack and closure to form the diester spiro adduct P_4, was investigated in greater detail. The largest observed K_2, from pH = 7 data, was assigned as the equilibrium constant for formation of P_4 from P_2. Thermodynamic reaction cycle calculations using this data and pK_1^P and pK_2^P allowed determination of the equilibria that exist between $P_1 \rightarrow P_4$ and $P_3 \rightarrow P_4$ respectively. Examination of the kinetics of the reverse reaction were enabled by synthetic preparation of P_4 under anhydrous conditions in acetonitrile. A freshly prepared solution of P_4 in acetonitrile was rapidly mixed with a 25-fold v/v excess of aqueous buffer at pH 5−9 utilizing a stopped-flow reaction apparatus. Progress curves were monitored by fluorescence detection and fit to double exponential equations. For this fitting, the slow rate was fixed to the k_{off} value for that pH obtained in Figure 6B. The rates thus obtained for the decomposition of P_4 are listed in Table 3. These data, when combined with the K_2 data obtained by ^{11}B NMR experiments, also enable the calculation of the forward reaction rates via the relationship $K_2 = k_4/k_{-4}$.

At this juncture, the similarities and differences of the reactions of benzoxaborole, **1**, and simple phenylboronic acid, **4**,[18] with **ARS** as a model diol are examined in order to assess any inherent benefit arising from the utilization of the benzoxaborole scaffold. The similarities include optimal binding at near neutral pH and a shared mechanistic scheme with the preferred route of reaction occurring between the singly deprotonated **ARS** (A_1) and the boronic form of **1** (B_1).

dx.doi.org/10.1021/jo302264g | J. Org. Chem. 2012, 77, 11200−11209

Table 3. Cyclization Step Reaction Rates vs pH[a]

	rate (s^{-1})	
pH	k_4	k_{-4}
5.0	0.26	0.65 ± 0.07
6.0	0.39	0.56 ± 0.09
7.0	0.20	0.23 ± 0.02
8.0	ND	0.18 ± 0.01
9.0	ND	0.99 ± 0.11

[a]The rate of the reverse reaction, k_{-4}, is obtained from observation of the rates of decomposition of synthetically prepared P_4 when rapidly mixed with aqueous buffer of various pH. The forward rate, k_4, is calculated using the relationship $K_2 = k_4/k_{-4}$. ND = not determined due to unavailability of K_2 measurements.

Differences can be found in both the steady-state and presteady-state. In the steady-state, there are the expected differences in binding vs pH due to the differing pK_a of **1** and **4**, Table 1. The optimal pH of binding for **1:ARS** is found to be between 6 and 7 while that for **4:ARS** was determined to be 7−8. At pH = 7, the overall association constant is about 25% greater for **1:ARS** vs **4:ARS**, 3200 and 2550 M^{-1}, respectively. Additionally, it is noted that the K_2 for **1:ARS** is greater at every pH for which the data is available, Figure 8.

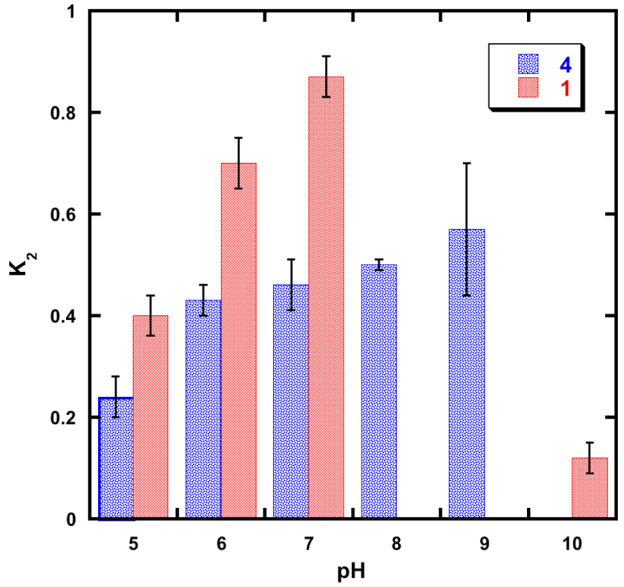

Figure 8. Comparison of the calculated K_2 values for the **1:ARS** (red) and **4:ARS** (blue)[18] reactions at pH 5−10. At all pHs for which data are available, the formation of the full-ester, spiro adduct by the benzoxaborole is preferred over the phenylboronic acid.

Comparison of the reactions in the presteady-state and the subsequent detailed reaction mechanisms illuminate the potential source of the increased reactivity/binding observed for the benzoxaborole scaffold. Examination of the individual rates given in Figure 7 with those determined for **4** do not show any striking differences, as might be expected for comparisons between two molecules with such similar structures. What is seen, however, is that the cyclization reaction for the formation of P_4 from **1** occurs at a slightly faster rate and that this product is more stable, as reflected in the greater K_2 values (Figure 8), than is observed for the reaction with **4**. For the **4:ARS** reaction, it was seen that the overall binding was dictated by K_{a1} with overall reaction K_a at pH 7 equal to K_{a1} for the middle path (2550 ± 95 and 2250 ± 250 M^{-1} s^{-1}, respectively). This type of simple reactivity was not observed for the **1:ARS** system where the contributions of both K_{a1} and K_2 needed to be accounted for (Table 2 and eq 3) to accurately replicate the binding of the overall reaction. In essence, it is believed that the relatively greater contribution of the diester adduct, P_4, to the overall reaction is responsible for the observed enhanced reactivity of the benzoxaborole scaffold.

This assertation was then tested by examining the reactions between **ARS** and several other compounds that are structurally related to both **1** and **4**, Figure 1. Compounds were selected to examine the roles that the oxaborole heterocycle (benzoxaborin, **2**, and 3,3-gem-dimethyl-benzoxaborole, **3**) and compound pK_a (4-trifluoromethyl-phenylboronic acid, **5**, and 5-methyl-benzoxaborole, **6**) might play in the reactivity of the benzoxaborole scaffold. These compounds' pK_a's were independently determined and are listed in Table 1. The reactions' kinetics were examined in the presteady-state after rapid mixing with a stopped-flow apparatus with an experimental setup nearly identical to that used above. The major difference in this case is that reaction progress was monitored via time-resolved, UV/vis spectral collection with photo diode array detection rather than fluorescence. This detection method was chosen to enhance the likelihood of reliably detecting contributions of the cyclic, diester product, P_4, that has been determined to have a much smaller fluorescence response than the intermediate, monoester product, P_2.

Separate solutions of **ARS** and the compounds **1**−**6** were prepared in matched aqueous buffer solutions at pH 6 and 8. In all cases, the final concentrations of **ARS** and **1**−**6** were 0.1 and 4 mM respectively after mixing. Data were collected for up to 100 s after mixing and the spectra from 350 to 700 nm were examined. Singular value decomposition (SVD) analysis was used to extract the number of detectable species, including intermediates, contributing to the observed reaction spectra. The resulting SVD basis vectors have been included in the Supporting Information.

In the case of a simple one-step reaction in which a spectral change is observed, two species corresponding to the reactant and product should be observed. Three species will be observed in the case of a two-step reaction in which the reactant, intermediate, and product have differing spectra. The results of these analyses on the reactions between **1**−**6** and **ARS** are summarized in Table 4. It can be seen that only compounds **1** and **6** exhibit three species in the reaction indicative of significant contributions to the reaction from intermediate and

Table 4. Number of Species Present in the Reaction between ARS and Various Boron Compounds as Determined by SVD Analysis of Time-resolved Reaction Spectra[a]

	boron compound					
pH	1	2	3	4	5	6
6	3	2	2	2	2	3
8	3	2	2	2	2	3

[a]Time-resolved UV/vis spectra (350-700 nm) were captured for the pre-steady state reactions of boron compounds **1**−**6** with **ARS** at pH 6 and 8. Singular value decomposition analysis revealed that only the compounds with an unsubstituted benzoxaborole heterocycle posses the signature, two-step reaction profile. SVD basis vectors for these designations are included in the Supporting Information.

dx.doi.org/10.1021/jo302264g | J. Org. Chem. 2012, 77, 11200−11209

product species. The simplest interpretation is that the rate of formation of the corresponding full ester, spiro adduct for **1** and **6**, relative to all other compounds, is competitive with the rate of intermediate formation so that three species, rather than two, are observed.

CONCLUSIONS

It has been observed that the benzoxaborole scaffold has been selected time and again for its enhanced reactivity or binding to target diols, whether on the cell surface or in the active site of an enzyme. Thus far, the rationale for its use seems to have arisen simply from phenomenological observations of its effectiveness when compared to other, similar compounds such as phenylboronic acid. In this work, we address the question "What properties of this scaffold are responsible for its unique reactivity?" by determining the mechanism of the reaction between benzoxaborole (**1**) and a model diol, **ARS**. Additionally, the reactivity of **1** is compared and contrasted with other structurally related compounds (**2**–**6**) in an attempt to pinpoint the structural source of these properties.

Experiments in the steady-state were executed to determine basic properties of benzoxaborole and the products formed in the reaction with **ARS** for comparison to those previously determined in the reaction between **ARS** and phenylboronic acid (**4**). As could be expected in the comparison of two compounds with such close structures, many similarities were found. These included general spectral (UV/vis, fluorescence) properties, responses to pH, and fluorescence lifetime measurements indicating two species contributing to the fluorescent signal. The major differences included a tighter binding observed for **1** with the maximum occurring at a lower solution pH. Also, greater formation of the diester, spiro adduct was observed at all pH conditions examined when compared with the previously determined data for **4**. Combined, these data confirm that the reaction is proceeding in two sequential steps.

Presteady-state analyses utilizing stopped-flow fluorescence spectrometry were used to elucidate a detailed mechanism for the reaction (Figure 7). This mechanism was found to parallel that determined for the reaction between **4** and **ARS** in our previous work. The preferred reaction occurs at near neutral pH between the singly deprotonated **ARS** and neutral, trigonal **1** ($\mathbf{A_1}$ and $\mathbf{B_1}$ respectively) to form the monoester adduct, $\mathbf{P_2}$, before intramolecular ring closure to the diester spiro adduct, $\mathbf{P_4}$. The reaction is much less favorable at either lower or higher solution pH. A key difference was noted in this system when the kinetic K_{a1} (k_{on}/k_{off}) was compared with the steady-state overall reaction K_a. In the reaction between **4** and **ARS**, K_{a1} was essentially identical to the overall K_a indicative of a system where the reaction is controlled by the initial association reaction. In the **1**:**ARS** system, the contributions of both K_{a1} and K_2 needed to be taken into account to reproduce the observed overall reaction K_a (eq 3).

Additionally, another difference between the systems was noted when the rate equations determined for **4**:**ARS** were applied to the benzoxaborole system. While the equation that describes the reverse reaction rates as a function of pH (eq 5) revealed an excellent fit to the k_{off} data, the forward reaction rate equation (eq 4) fit the k_{on} data poorly at pH < 6 (Figure 6). These data, however, revealed an apparent pK_a that depended on the ionization of the intermediate product ($P_1 \rightarrow P_2$) rather than on the ionization of any of the reactants. This result was taken as further evidence for the significant contribution of the intramolecular cyclization step in the overall reaction course. Indeed, it is proposed that this kinetically competitive cyclization step is the source of the enhanced reactivity of the benzoxaborole heterocycle.

Finally, a stopped-flow method that obtains time-resolved UV/vis spectra of the reaction was used for identification of readily formed reaction intermediates. This method allows the rapid comparison of the reactivity of several structurally related compounds. These experiments compared the effects of modifications to the benzoxaborole heterocycle and compound pK_a (from distal aromatic ring substitutions) on the compounds' reactivities. Based on these results, it appears that the five-membered oxaborole ring itself is a major contributor to the unique reactivity observed with the benzoxaborole scaffold. It is proposed that the reactivity arises from the geometry about the neutral, trigonal planar boron atom when it is constrained in a five-membered ring. This ring strain is alleviated when the boron atom forms an anionic, tetrahedral species by either hydroxlyation (conjugate base formation) or diesterification (i.e., formation of the spiro P_4 species). These results may now provide a basis for further improvements to this scaffold and a rationale for the expanded use of this cyclic boronate in applications ranging from drug discovery to synthetic protocols.

EXPERIMENTAL SECTION

Common solvents and reagents were obtained from commercial sources and were of the highest available purity. 2-(Hydroxymethyl)-benzene boronic acid cyclic monoester (benzoxaborole, **1**) was purchased from Lancaster Synthesis, Inc. and purified by silica gel column chromatography with 25% ethyl acetate in hexanes. 2-(2-hydroxyethyl)benzene boronic acid cyclic monoester (benzoxaborin, **2**) and 3,3-*gem*-dimethyl-benzoxaborole (**3**) were provided by Scynexis, Inc. 5-Methyl-benzoxaborole (**6**) was provided by Anacor Pharmaceuticals, Inc. **ARS** and all buffer solutions were prepared with double-deionized water in triple-rinsed, acid-washed glassware. The **ARS** stock solution was 10 mM and was protected from light. All aqueous solutions were filtered through 0.45 μm Supor syringe filters from Pall Life Sciences. Stock solutions of **1**–**6** were 200 mM in DMSO. All solutions were stored at 4 °C in polypropylene tubes. Unless otherwise noted, all data were plotted and analyzed using KaleidaGraph v3.5 by Synergy Software.

Buffers were prepared as 500 mM stock solutions and adjusted to final pH as indicated with either HCl or NaOH: Glycine (pH = 3.0 and 3.5), Acetic acid-Sodium Acetate (pH = 4.0, 4.5 and 5.0), MES (pH = 5.5, 6.0, and 6.5), HEPES (pH = 7.0, 7.5, and 8.0), CHES (pH = 8.6, 9.0, 9.5, and 10.0), and CAPS (pH = 10.5 and 11.0). Final solution pH was determined by preparing mock solutions (5 mL, lacking only compounds) and measuring pH with a pH meter calibrated against aqueous buffer solutions using a combination electrode without correction for liquid junction potentials.

UV/Visible Spectra Collection. Solutions were placed into 1 mL, 1 cm path length quartz cuvettes and spectral scans (1 nm resolution) were taken at room temperature. Scans were taken in the following regions: 240–340 nm for **1**–**6**; 240–700 nm for **ARS**; 350–700 nm for **1**:**ARS**. Solutions consisted of 1 mM **1**, 100 μM **ARS**, or 8 mM **1** and 100 μM **ARS**, respectively. All solutions contained either 0.5% or 4% v/v DMSO and any one of 100 mM HCl, 100 mM NaOH, or 50 mM buffer. Ionization constants were derived from these data by the method of Tomsho, et al.[7]

Fluorescence Spectra Collection. Measurements were collected at room temperature. Emission scans were taken from 460 to 800 nm with an excitation wavelength of 440 nm. Excitation scans were then taken from 300 to 550 nm with an emission wavelength equal to the wavelength of maximum fluorescence determined in the emission scan. All slit widths were set to 2 nm. Solutions consisted of 20 μM **ARS**, 4% v/v DMSO, 0 or 2 mM **1**, and any one of 100 mM HCl, 100 mM NaOH, or 50 mM buffer.

dx.doi.org/10.1021/jo302264g | J. Org. Chem. 2012, 77, 11200–11209

Fluorescence Lifetime (TCSPC) Determination. Data were collected at room temperature with a NanoLED-495 excitation source (1 MHz refresh rate) while the emission wavelength was set to 590 nm (20 nm bandpass). Data were collected with Data Station v. 2.5 and analysis was done with DAS6 software. Solutions consisted of 20 μM **ARS**, 2 mM **1**, 4% v/v DMSO, and 50 mM buffer (pH 4−10). Ludox CL colloidal silica solutions were used as light scattering standards.

Steady State Fluorescence Titrations. Measurements were collected at 25.0 °C with excitation at 460 nm and emission at 590 nm utilizing 5 nm slit widths. The K_a of the **1**:**ARS** complex was determined by two-component fluorescent titrations by the method of Springsteen and Wang.[22] The K_a values were determined by fitting the data to eq 2. These samples contained 50 mM buffer, 5% v/v DMSO, 20 μM **ARS**, and 0−10 mM **1** in ddH_2O. An **ARS** solution and solutions of all other components except for **ARS** were prepared and equilibrated at 25.0 °C in separate vessels. Upon **ARS** solution addition, the complete reaction solution was mixed well and maintained in the dark at 25.0 °C for 3 min prior to the measurement of fluorescence.

Isothermal Titration Calorimetry. A solution consisting of 0.4 mM **ARS** was titrated with 8 mM **1**, both solutions also contained 50 mM HEPES at pH 7 and 4% v/v DMSO in ddH_2O. A blank titration of **1** into buffer lacking **ARS** was done to correct for the heat of dilution of the solution of **1**. The cell temperature was held to 25.0 °C, injection volume was 10 μL, and injection duration and spacing were 24 and 240 s respectively. After correction for heat of dilution of **1**, the data were fit to a one-site binding model using MicroCal Origin 5.0 for ITC software package. From these data, the association constant and thermodynamic parameters of the reaction were determined.

^{11}B-NMR. Spectra were collected at 96.21 MHz using a 4.9 μs 90° pulse, 488 ms FID acquisition time, and a 1 s acquisition delay. The sweep width was set to 87.2 ppm and the temperature to 25.0 °C. All chemical shifts were referenced to an external standard of $BF_3(Et_2O)$ at 0.0 ppm. Samples were prepared in 5% v/v DMSO and 10% v/v D_2O in ddH_2O as the lock solvent and were placed into quartz NMR tubes. Each sample consisted of 50 mM buffer, 10 mM boron compound **1**, and 7.5 mM **ARS**. Two thousand scans were taken for each sample and the data were then processed using SpinWorks v2.5.5. A minimum of three independent determinations were made at each pH examined from 5 to 10.

Preparation of the 1:ARS Full-ester Adduct (P_4). Using standard procedures to exclude moisture, Alizarin Red S (173 mg, 0.5 mmol), benzoxaborole (74 mg, 0.5 mmol), and anhydrous potassium carbonate (173 mg, 1.25 mmol) are sealed in a round-bottomed flask under an argon atmosphere. To this is added 10 mL of acetonitrile (dried by stirring over anhydrous potassium carbonate under argon) and the resulting suspension is stirred vigorously for ∼18 h at room temperature in the dark. Stirring is stopped and the suspension is allowed to settle. Using dry needles, syringes, and syringe filters, the supernatant was removed and filtered through a 0.45 μm nylon syringe filter taking care to minimize solution exposure to air. The solution was protected from light and used immediately. ^{1}H NMR (CD_3CN) δ: 8.25 (m, 2H), 8.02 (s, 1H), 7.92 (m, 2H), 7.77 (d, 1H*), 7.45 (m, 3H*), 6.78 (br s, 1H*), 5.06 (s, 2H*). ^{11}B-NMR (CD_3CN) δ: 32.3 (1.00), 16.3 (0.020), 8.2 (0.025); MS ESI- m/z (relative intensity) $[M]^{-2}$ 217.0 (50.3%), $[M + K]^{-2}$ 237.5 (13.5%), $[ARS]^-$ 318.9 (100%), $[M]^-$ 434.9 (90.2), $[M + K]^-$ 473.0 (14.7%); λ_{max} (CH_3CN) 460 nm. *these protons are attributed to **1** and are labeled according to the number present in the product molecule for clarity; however an approximately 17-fold excess is observed in the reaction due to the limited solubility of **ARS**.

Presteady State Kinetics. *(1). Forward Reaction Kinetic Determinations with Fluorescence Detection.* Reaction progress was monitored utilizing a stopped-flow reaction analyzer with fluorescence detection. The excitation wavelength was 450 nm with a 4.65 nm slit width, emission was monitored with the use of an OG530 nm long wave pass filter, temperature was controlled at 25.0 ± 0.1 °C, and reaction progress was followed for up to 100 s. For each pH and **ARS** concentration examined, two solution sets were prepared such that all contained 50 mM buffer and 4% v/v DMSO in ddH_2O. The **ARS** solution additionally contained 0.02−0.20 mM **ARS** while the boron compound solutions contained 2 mM **1**; in both cases, the final concentrations of both **ARS** and **1** are halved upon mixing for reaction initiation. Reaction progress curves were analyzed using the Applied Photophysics Pro-Data Viewer v. 4.2.0 for fitting to a single exponential curve to obtain apparent rate data.

(2). Reverse Reaction Kinetic Determinations. The stopped-flow instrumental setup was as detailed for the forward reaction kinetic determinations above except the instrument was configured for asymmetric mixing with a ratio of 1:25 and data collection up to 60 s. The **1**:**ARS** full-ester adduct solution in acetonitrile is freshly prepared as described above. Buffer solutions, 50 mM in ddH_2O, of the desired pH (5−9) are prepared. Mixing for reaction initiation results in a 25-fold dilution of the **1**:**ARS** full-ester adduct solution into buffer resulting in 4% v/v acetonitrile final. Reaction progress curves were analyzed using the Applied Photophysics Pro-Data Viewer v. 4.2.0 for fitting to a double exponential curve to obtain apparent rate data.

(3). UV/vis Kinetic Determinations with Photo Diode Array Detection. The stopped-flow instrumental setup was as detailed for the forward reaction kinetic determinations above except the instrument was configured for photo diode array detection of the UV/vis spectra. The light source utilized was a xenon short arc lamp with the diffraction grating of the monochromator taken out of line and 14 nm slits. Path length was 1 cm and blanks were taken on mock reaction solutions lacking only boron compounds and **ARS**. For each pH examined, two solution sets were prepared such that all contained 50 mM buffer and 4% v/v DMSO in ddH_2O. The **ARS** solution additionally contained 0.20 mM **ARS** while the boron compound solutions contained 8 mM **1**−**6**; in both cases the final concentrations of both the **ARS** and boron compounds are halved upon mixing for reaction initiation. Time resolved reaction spectra from 350 to 700 nm were analyzed using the Applied Photophysics ProK Global Analysis v. 1.0.8 software for SVD analysis and fitting to either one- or two-step reaction mechanism models.

■ ASSOCIATED CONTENT

Supporting Information

Spectral data for the pK_a determinations of **1**, **ARS**, and the **1**:**ARS** complex; NMR and MS spectra for the synthesis of the **1**:**ARS** diester adduct in acetonitrile; ^{11}B NMR integration data and K_2 calculation; KinTek modeling results; SVD basis vectors for **1**−**6** at pH 6 and 8. This material is available free of charge via the Internet at http://pubs.acs.org.

■ AUTHOR INFORMATION

Corresponding Author

*Tel: 814-865-2882. Fax: 814-865-2973. E-mail: sjb1@psu.edu.

Present Address

†Department of Chemistry and Biochemistry, University of the Sciences in Philadelphia, 600 South 43rd St., Philadelphia, PA 19104.

Notes

The authors declare no competing financial interest.

■ ACKNOWLEDGMENTS

We thank Dr. C. Tony Liu for critical review of the manuscript; Anacor Pharmaceuticals, Inc. of Palo Alto, CA, for providing a sample of compound **6**; and Scynexis, Inc. of Research Triangle Park, NC, for providing samples of compounds **2** and **3**.

■ REFERENCES

(1) Torssell, K. *Ark. Kemi* **1957**, *10*, 507−511.

(2) Li, X.; Zhang, Y.-K.; Liu, Y.; Ding, C. Z.; Li, Q.; Zhou, Y.; Plattner, J. J.; Baker, S. J.; Qian, X.; Fan, D.; Liao, L.; Ni, Z.-J.; White, G. V.; Mordaunt, J. E.; Lazarides, L. X.; Slater, M. J.; Jarvest, R. L.; Thommes, P.; Ellis, M.; Edge, C. M.; Hubbard, J. A.; Somers, D.;

Rowland, P.; Nassau, P.; McDowell, B.; Skarzynski, T. J.; Kazmierski, W. M.; Grimes, R. M.; Wright, L. L.; Smith, G. K.; Zou, W.; Wright, J.; Pennicott, L. E. *Bioorg. Med. Chem. Lett.* **2010**, *20*, 3550−3556.
(3) Dixon, D. D.; Lockner, J. W.; Zhou, Q.; Baran, P. S. *J. Am. Chem. Soc.* **2012**, *134*, 8432−8435.
(4) Snyder, H. R.; Reedy, A. J.; Lennarz, W. J. *J. Am. Chem. Soc.* **1958**, *80*, 835−838.
(5) Dowlut, M.; Hall, D. G. *J. Am. Chem. Soc.* **2006**, *128*, 4226−4227.
(6) Bérubé, M.; Dowlut, M.; Hall, D. G. *J. Org. Chem.* **2008**, *73*, 6471−6479.
(7) Tomsho, J. W.; Pal, A.; Hall, D. G.; Benkovic, S. J. *ACS Med. Chem. Lett.* **2012**, *3*, 48−52.
(8) Adamczyk-Woźniak, A.; Cyrański, M. K.; Żubrowska, A.; Sporzyński, A. *J. Organomet. Chem.* **2009**, *694*, 3533−3541.
(9) Baker, S. J.; Tomsho, J. W.; Benkovic, S. J. *Chem. Soc. Rev.* **2011**, *40*, 4279−4285.
(10) Rock, F. L.; Mao, W.; Yaremchuk, A.; Tukalo, M.; Crepin, T.; Zhou, H.; Zhang, Y. K.; Hernandez, V.; Akama, T.; Baker, S. J.; Plattner, J. J.; Shapiro, L.; Martinis, S. A.; Benkovic, S. J.; Cusack, S.; Alley, M. R. K. *Science* **2007**, *316*, 1759−1761.
(11) Obrecht, D.; Bernardini, G.; Dale, G.; Dembowsky, K. In *Annual Reports in Medicinal Chemistry*; Elsevier Inc.: New York, 2011; Vol. *46*, pp 245−262.
(12) Ding, D.; Meng, Q.; Gao, G.; Zhao, Y.; Wang, Q.; Nare, B.; Jacobs, R.; Rock, F.; Alley, M. R. K.; Plattner, J. J.; Chen, G.; Li, D.; Zhou, H. *J. Med. Chem.* **2011**, *54*, 1276−1287.
(13) Qiao, Z.; Wang, Q.; Zhang, F.; Wang, Z.; Bowling, T.; Nare, B.; Jacobs, R. T.; Zhang, J.; Ding, D.; Liu, Y.; Zhou, H. *J. Med. Chem.* **2012**, *55*, 3553−3557.
(14) Akama, T.; Baker, S. J.; Zhang, Y.-K.; Hernandez, V.; Zhou, H.; Sanders, V.; Freund, Y.; Kimura, R.; Maples, K. R.; Plattner, J. J. *Bioorg. Med. Chem. Lett.* **2009**, *19*, 2129−2132.
(15) Xia, Y.; Cao, K.; Zhou, Y.; Alley, M. R. K.; Rock, F.; Mohan, M.; Meewan, M.; Baker, S. J.; Lux, S.; Ding, C. Z.; Jia, G.; Kully, M.; Plattner, J. J. *Bioorg. Med. Chem. Lett.* **2011**, *21*, 2533−2536.
(16) Kim, H.; Kang, Y. J.; Kang, S.; Kim, K. T. *J. Am. Chem. Soc.* **2012**, *134*, 4030−4033.
(17) Ellis, G. A.; Palte, M. J.; Raines, R. T. *J. Am. Chem. Soc.* **2012**, *134*, 3631−3634.
(18) Tomsho, J. W.; Benkovic, S. J. *J. Org. Chem.* **2012**, *77*, 2098−2106.
(19) Huebner, A.; Qu, Z. W.; Englert, U.; Bolte, M.; Lerner, H. W.; Holthausen, M. C.; Wagner, M. J. *J. Am. Chem. Soc.* **2011**, *133*, 4596−4609.
(20) DiCesare, N.; Lakowicz, J. R. *J. Phys. Chem. A* **2001**, *105*, 6834−6840.
(21) Yoon, J.; Czarnik, A. W. *J. Am. Chem. Soc.* **1992**, *114*, 5874−5875.
(22) Springsteen, G. *Tetrahedron* **2002**, *58*, 5291−5300.